LETTERS
DOI: 10.1038/s41564-017-0033-2
nature microbiology

Evolution of host adaptation in the *Salmonella* typhoid toxin

Xiang Gao[1], Lingquan Deng[2,4], Gabrielle Stack[1], Hai Yu[3], Xi Chen[3], Yuko Naito-Matsui[2], Ajit Varki[2] and Jorge E. Galán[1*]

The evolution of virulence traits is central for the emergence or re-emergence of microbial pathogens and for their adaptation to a specific host[1–5]. Typhoid toxin is an essential virulence factor of the human-adapted bacterial pathogen *Salmonella* Typhi[6,7], the cause of typhoid fever in humans[8–12]. Typhoid toxin has a unique A_2B_5 architecture with two covalently linked enzymatic 'A' subunits, PltA and CdtB, associated with a homopentameric 'B' subunit made up of PltB, which has binding specificity for the *N*-acetylneuraminic acid (Neu5Ac) sialoglycans[6,13] prominently present in humans[14]. Here, we examine the functional and structural relationship between typhoid toxin and ArtAB, an evolutionarily related AB_5 toxin encoded by the broad-host *Salmonella* Typhimurium[15]. We find that ArtA and ArtB, homologues of PltA and PltB, can form a functional complex with the typhoid toxin CdtB subunit after substitution of a single amino acid in ArtA, while ArtB can form a functional complex with wild-type PltA and CdtB. We also found that, after addition of a single-terminal Cys residue, a CdtB homologue from cytolethal distending toxin can form a functional complex with ArtA and ArtB. In line with the broad host specificity of *S.* Typhimurium, we found that ArtB binds human glycans, terminated in *N*-acetylneuraminic acid, as well as glycans terminated in *N*-glycolylneuraminic acid (Neu5Gc), which are expressed in most other mammals[14]. The atomic structure of ArtB bound to its receptor shows the presence of an additional glycan-binding site, which broadens its binding specificity. Despite equivalent toxicity in vitro, we found that the ArtB/PltA/CdtB chimaeric toxin exhibits reduced lethality in an animal model, indicating that the host specialization of typhoid toxin has optimized its targeting mechanisms to the human host. This is a remarkable example of a toxin evolving to broaden its enzymatic activities and adapt to a specific host.

Typhoid toxin appears to have evolved through the combination of two 'A' subunits that are independently present in other bacterial toxins into a single toxin[7]. PltA exhibits significant amino-acid sequence similarity to the ADP-ribosyl transferases that serve as A subunits in several AB_5 exotoxins, while CdtB is a homologue of the A subunit of the cytolethal distending toxins (CDT) encoded by several bacterial pathogens[16] (Fig. 1a and Supplementary Fig. 1). CdtB and PltA are linked together by a single disulfide bond coordinated by uniquely positioned cysteine residues (Fig. 1a and Supplementary Fig. 1)[6]. The crystal structure of the typhoid toxin shows that the atomic interface between CdtB and PltA is rather limited, and reduction of the disulfide bond results in dissociation of the complex[6]. Despite the very high amino-acid sequence similarity of CdtB and PltA with their homologues in other bacteria, the Cys residues involved in tethering them to form typhoid toxin are unique to these two subunits (Fig. 1a and Supplementary Fig. 1). These observations suggest that the evolution of this multi-subunit toxin is likely to be relatively recent. In support of this hypothesis, homologues of each of the components of typhoid toxin are encoded within various *Salmonella enterica* subspecies as components of other toxins[17,18]. For example, available genome sequencing data indicate the presence of an intact locus encoding all the CDT components, including CdtB in *Salmonella* Arizonae and Diarizonae[18]. Furthermore, certain strains of *S.* Typhimurium encode the toxin ArtAB, which exhibits very significant amino-acid sequence similarity to the PltA and PltB components of typhoid toxin (Fig. 1a and Supplementary Figs. 1 and 2)[15]. A degraded copy of the *artAB* locus is present in several *S. enterica* serovars[15]. Because *Salmonella* can readily exchange genetic materials across different serovars and strains, the presence of the different components of typhoid toxin in different *Salmonella* lineages, sometimes within mobile genetic elements, provides a framework through which typhoid toxin could have emerged.

We therefore investigated the potential evolutionary relatedness between ArtAB and typhoid toxin. We introduced a Cys residue in ArtA ($ArtA^{R214C}$) at the equivalent position of the Cys residue in PltA ($PltA^{C214}$) that forms a disulfide bond with CdtB, co-expressed it with ArtB and CdtB, and examined their ability to form a complex. We found that ArtB, $ArtA^{R214C}$ and CdtB formed a complex in the predicted stoichiometry of 5:1:1 (Fig. 1b,c). Importantly, addition of a reducing agent resulted in the dissociation of CdtB from ArtA (Fig. 1b,c), demonstrating that the assembled complex has an equivalent architecture to that of typhoid toxin. We then tested the ability of the 'B' subunit ArtB to form a complex with PltA and CdtB, the two A subunits from typhoid toxin. We found that co-expression of all these components led to the assembly of a stable complex of a size consistent with that of an $ArtB_5$–PltA–CdtB complex (Fig. 1d and Supplementary Fig. 3). We then examined the functionality of the resulting chimaeric toxins by testing their CdtB-dependent toxicity when applied to cultured cells. We found that, consistent with the formation of stable complexes (Supplementary Fig. 4), the CdtB-dependent toxic activity of the different chimaeric toxins was similar to that of typhoid toxin (Fig. 1e). We also examined the ability of a homologue of CdtB from the *S. diarizonae* CDT to form a complex with ArtA and ArtB (Fig. 1e). We found that, after addition of single Cys residue as its last amino acid, $CdtB^{Cys276}$ was able to form a functional complex with ArtA and ArtB (Fig. 1e). Taken together, these results demonstrate a very close structural

[1]Department of Microbial Pathogenesis, Yale University School of Medicine, New Haven, CT 06536, USA. [2]Glycobiology Research and Training Center, Departments of Medicine, Pathology and Cellular and Molecular Medicine, University of California San Diego, La Jolla, CA 92093, USA. [3]Department of Chemistry, University of California Davis, Davis, CA 95616, USA. Present address: [4]GlycoMimetics, Inc., 9708 Medical Center Drive, Rockville, MD 20850, USA. *e-mail: jorge.galan@yale.edu

relationship among the components of these evolutionary related toxins and, more importantly, a remarkable plasticity to form functional chimaeric complexes, which probably facilitates the evolution of this toxin family.

Typhoid toxin exhibits exquisite preference for human-enriched Neu5Ac-terminated sialoglycans on surface glycoproteins, which serve as its receptors[13]. The amino-acid sequence similarity between PltB and ArtB (Supplementary Fig. 2) suggests that the ArtB may

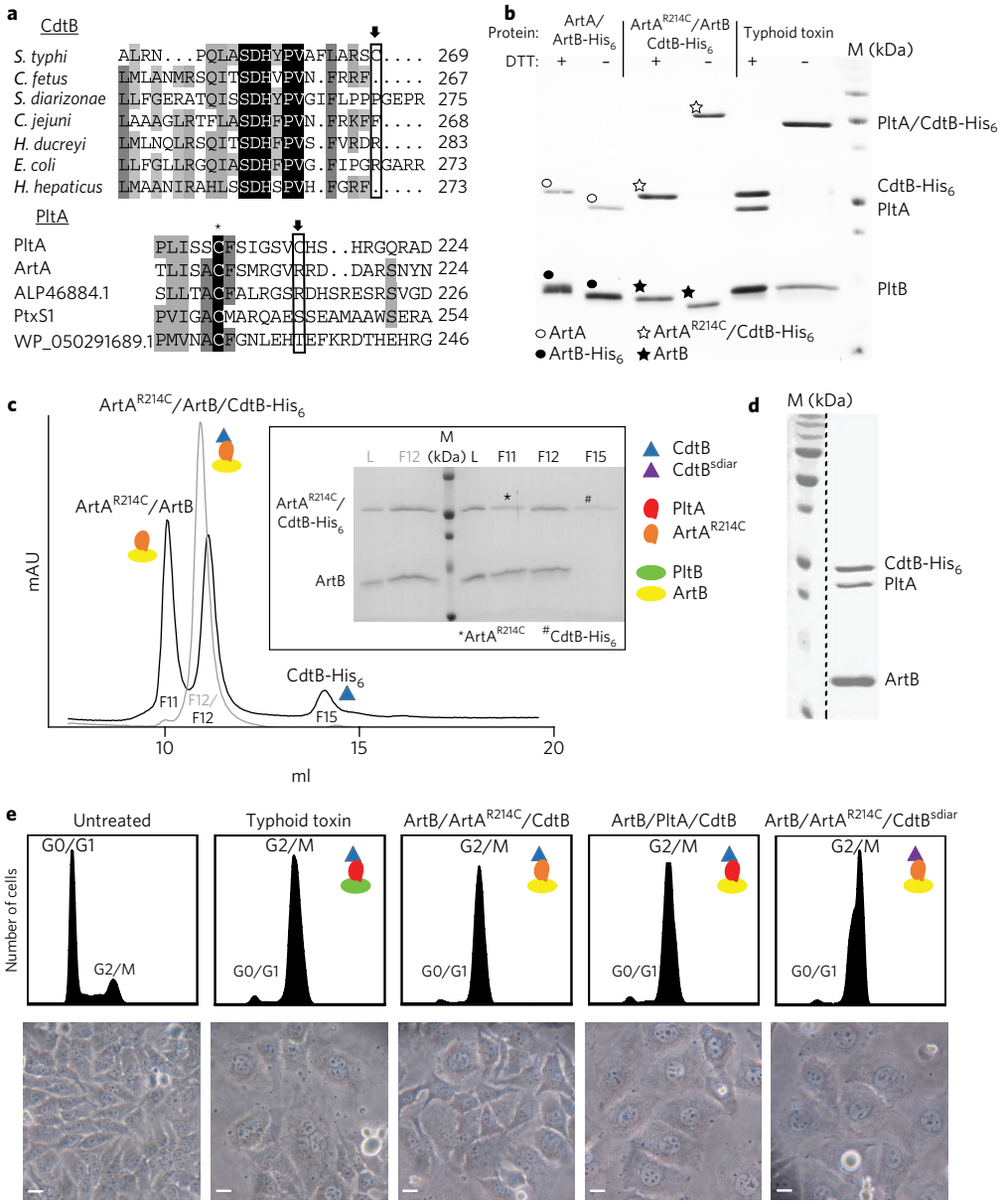

Fig. 1 | The ArtAB toxin components can form a functional complex with typhoid toxin subunits. a, Amino-acid sequence comparison of CdtB and PltA homologues. Conserved and unique cysteines are indicated with an asterisk and an arrow, respectively. ALP46884.1 and WP_050291689.1 are PltA homologues from *Escherichia coli* and *Yersinia kristensenii*, respectively. PltxS1 is the A subunit from pertussis toxin. **b**, Purified ArtB/ArtA, ArtB/ArtA^{R214C}/CdtB or typhoid toxin (PltB/PltA/CdtB) protein complexes were analysed by SDS–PAGE in the presence or absence of dithiothreitol (DTT) to release CdtB, which is linked to the complex by a disulfide bond. The migration of ArtA and His$_6$-tagged CdtB are very similar in SDS–PAGE, so in the presence of DTT the two bands overlap. In the absence of DTT, ArtA and CdtB (like CdtB and PltA in the case of typhoid toxin, see right lanes) migrate as a single, slower moving band, an indication that these subunits are linked by a disulfide bond. Open circles, ArtA; filled circles, ArtB-His$_6$; open stars, ArtA^{R214C}/CdtB-His$_6$; filled stars, ArtB. This experiment was carried out twice with equivalent results. **c**, The ArtA^{R214C}/ArtB/CdtB chimaeric toxin complex was analysed by ion exchange chromatography before (grey line) and after (black line) treatment with DTT. L, loading control; M, molecular weight markers; F, chromatographic fractions. Inset: SDS–PAGE analyses of the indicated chromatographic fractions. *ArtA^{R214C}; #CdtB-His$_6$. This experiment was carried out once. **d**, ArtB can form a complex with wild-type PltA and CdtB. The ArtB/PltA/CdtB complex was purified by ion exchange and size exclusion chromatography and subsequently analysed by SDS–PAGE and Coomassie blue staining. This experiment was carried out three times with equivalent results. The dashed black line indicates that this panel is a composite image of two discontinuous lanes from the same gel. **e**, Toxicity of the chimaeric toxin complexes. Cultured Henle-407 epithelial cells were treated with typhoid toxin (3.5 pM), ArtB/ArtA^{R214A}/CdtB (15 pM), ArtB/PltA/CdtB (15 pM) or ArtB/ArtA^{R214A}/CdtB^{sdiar}, and the CdtB-mediated cell cycle arrest was assayed by flow cytometric analysis. CdtB^{sdiar}: CdtB from *S. diarizonae*. Light microscopic images of mock or toxin-treated cells are also shown. Scale bars, 50 μm. This experiment was carried out three times with equivalent results.

also bind sialoglycans. Consistent with this hypothesis, removal of surface sialic acids from cultured cells reduced ArtB binding (Fig. 2a and Supplementary Fig. 5). Because ArtAB is encoded by the broad-host-range *S.* Typhimurium, we hypothesized that the binding specificity of ArtB may differ from that of the human-adapted typhoid toxin. To test this hypothesis we probed the ability of fluorescently labelled ArtB to bind a diverse group of glycans arrayed on a solid surface. We found that, similar to typhoid toxin, ArtB was able to bind a diverse group of sialylated glycans with the consensus structure Neu5Acα2-3Galβ1-3/-4Glc/GlcNAc (Fig. 2b and Supplementary Table 1). ArtB was also able to bind an additional group of sialylated glycans with the consensus

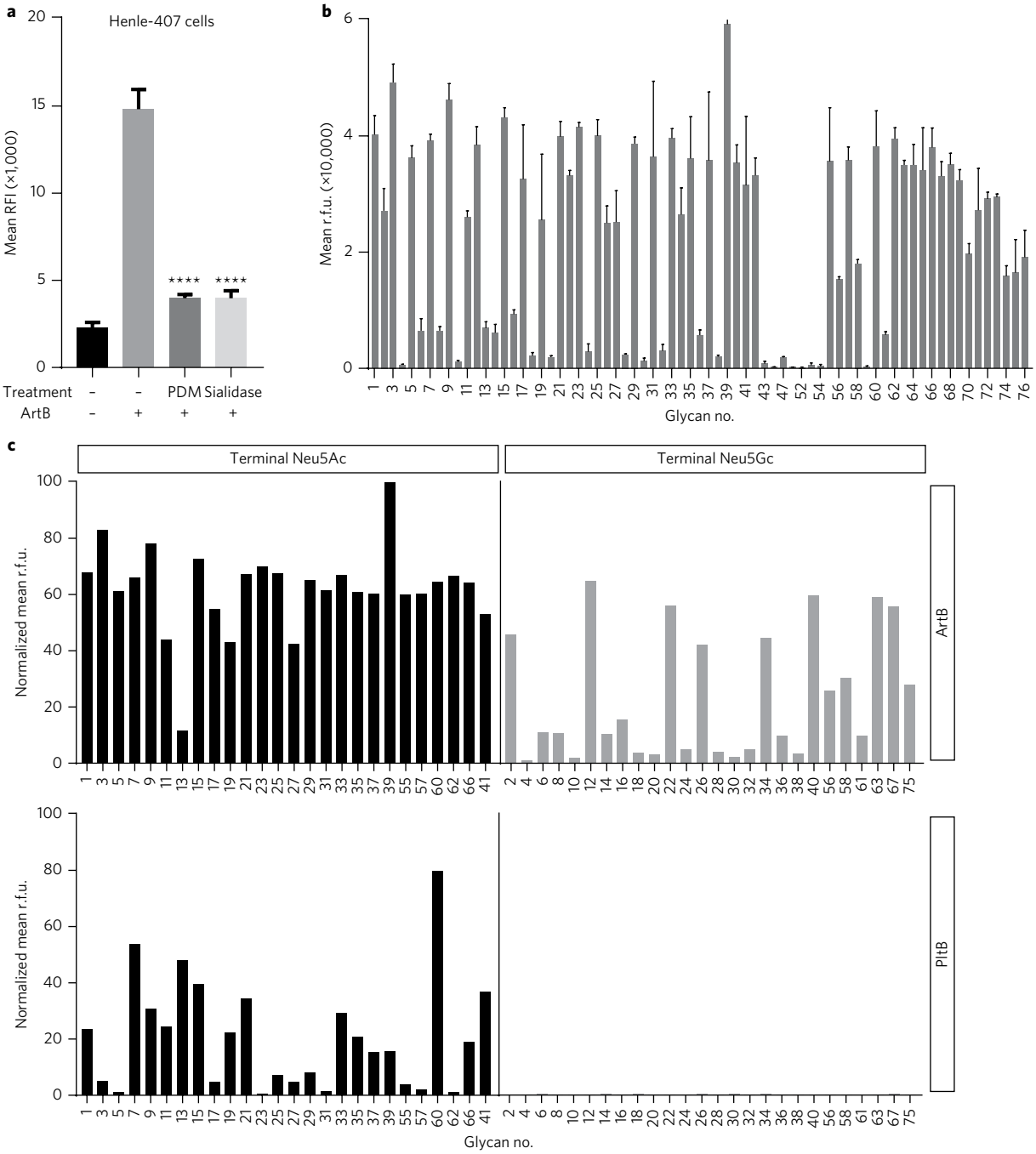

Fig. 2 | ArtB binds Neu5Ac- and Neu5Gc-terminated glycans. a, Removal of surface glycans reduces ArtB binding to cultured cells. Henle-407 cells were treated with a mixture of glycosidases (PDM, protein deglycosylation mix) or a sialidase (α2-3/6/8-neuraminidase) and the ability of treated and control cells to bind fluorescently labelled ArtB (2.5 μM) was evaluated by flow cytometry. The *y*-axis values represent relative fluorescence intensity (RFI). Bars represent mean ± s.d. of at least three independent measurements. Two-tailed Student's *t*-tests were performed to determine the statistical significance for two group comparisons. ****$P < 0.0001$, compared to the RFI of ArtB-binding to the untreated cells. **b**, ArtB-binding to a customized glycan microarray. The *y*-axis values represent average and standard deviation of the relative fluorescence units (r.f.u.) from four independent experiments, and the *x*-axis indicates glycan numbers (Supplementary Table 1). **c**, Comparison of ArtB-binding to paired Neu5Ac- and Neu5Gc- terminated glycans. The *y*-axis values represent the normalized average r.f.u. from four independent experiments and the *x*-axis indicates glycan numbers (Supplementary Table 2).

Neu5Acα2-6Gal/GalNAc, which typhoid toxin did not (Fig. 2b and Supplementary Table 1). Importantly, however, unlike typhoid toxin, ArtB was also able to bind Neu5Gc-terminated glycans (Fig. 2c and Supplementary Table 2). The broad binding specificity of ArtB is entirely consistent with the broad host range of the *S. enterica* serovar that harbours it.

We have previously shown that a single amino-acid substitution in the glycan-binding site of PltB (PltB^{S35A}) completely abolishes the ability of typhoid toxin to bind its glycan receptors and to intoxicate human cells[6]. However, we found that, in contrast to PltB, the equivalent mutation in ArtB (ArtB^{S31A}) retained a significant ability to bind cultured cells (Supplementary Fig. 6). These results suggested substantial differences between the mechanisms of glycan binding in ArtB and PltB. To gain insight into the structural basis for the binding specificity of ArtB, we determined its atomic structures alone (at 2.3 Å resolution, Fig. 3a) or bound to its glycan receptor Neu5Acα2-3Galβ1-4Glc (at 2.2 Å resolution, Fig. 3b and Supplementary Table 3). For comparison, we also solved the structure of PltB bound to the same glycan (Fig. 3c). In the crystal, each asymmetric unit of ArtB contained 10 molecules organized into two homopentamers, as predicted by its homology to other AB_5 toxins. In each of the pentamers, the ArtB protomer shows a typical oligosaccharide-binding fold located on the side of the pentamer, which corresponds to the equivalent binding site observed in the PltB structure. Clear electron density corresponding to the Neu5Acα2-3Galβ was observed at this site in two of the five subunits of the ArtB and in three of the PltB pentamers (Fig. 3a–c). The other sites were occupied by 2-(*N*-morpholino)ethanesulfonic acid (present in the crystallization buffer), which exhibits a similar structure to Neu5Ac. A close-up view of the ArtB canonical glycan-binding site shows that the Neu5Ac moiety interacts through multiple direct hydrogen bonds and water-mediated hydrogen bonds with Asn27, Tyr29, Gln30, Ser31, Arg59 and Asn65 in ArtB (Fig. 3d). In addition, the Neu5Ac ring makes a hydrophobic contact with the aromatic ring of Tyr29. Overall, the arrangement of Neu5Ac and the interactions between Neu5Ac and ArtB are very similar to what is seen in PltB, which makes contact with the glycan moiety with an equivalent interaction involving Tyr33, Tyr34, Ser35, Lys59 and Thr65 (Supplementary Fig. 7). However, ArtB has a Tyr103 that is absent from PltB (Fig. 3d). The corresponding residue in the related toxin SubB has been shown to form a critical hydrogen bond with the extra hydroxyl group of Neu5Gc[19]. This structural feature is consistent with the observation that ArtB, like SubB, can also bind glycans terminated with Neu5Gc.

Surprisingly, an additional unambiguous glycan density was detected away from the predicted glycan-binding site of the ArtB pentamer in three or four out of the five protomers in different pentamers (Fig. 3b). No glycan density was detected at an equivalent position of PltB. At this additional glycan-binding site, ArtB makes contact with both the Neu5Ac and Gal moieties in Neu5Acα2-3Galβ 1-4Glc through multiple interactions. For example, Ser45, Gly46, Phe75, Gly76, Lys79, Val107, Thr109 and Asp110 interact with the Neu5Ac moiety through multiple direct hydrogen bonds and water-mediated hydrogen bonds. In addition, the aromatic ring of Phe75 makes hydrophobic contact with the ring structure of Neu5Ac, and Thr109 makes contact with the Gal moiety of Neu5Acα2-3Galβ 1-4Glc through hydrogen bonding (Fig. 3e). Comparison of this additional glycan-binding site in ArtB with the equivalent surface in PltB reveals the presence in ArtB of a spoon-like structure critical for ligand binding, which is absent in PltB (Fig. 3f). Amino-acid sequence alignment of this region of ArtB with the equivalent region in PltB showed the presence of a unique five-amino-acid insertion in ArtB (Fig. 3g), which is responsible for the structural features associated with glycan binding. Comparison of the atomic structures of the receptor-bound and apo forms of ArtB indicates that, similar to PltB, binding to its glycan receptors does not result in detectable conformational changes (Supplementary Figs. 8 and 9). Taken together, these findings indicate that ArtB has an additional glycan-binding site that may contribute to its expanded glycan-binding repertoire and that may have been eliminated from typhoid toxin by the introduction of a small deletion during the process of its adaptation to humans.

The residual glycan-binding activity of the ArtB^{S31A} mutant coupled to the finding of a second glycan-binding site in ArtB prompted us to explore the potential specific contribution of each one of these sites to its overall glycan-binding activity. We generated and purified ArtB^{S31A}, ArtB^{S45A} single mutants as well as ArtB$^{S31A/S45A}$ double mutant proteins (Supplementary Fig. 10) and compared their ability to bind cultured epithelial cells. We found that, in comparison to wild-type ArtB, the binding of ArtB^{S31A} and ArtB^{S45A} was reduced but not abrogated. In contrast, the binding of the ArtB$^{S31A/S45A}$ double mutant was undetectable (Supplementary Fig. 11). These observations suggest that both sites contribute to ArtB binding to cultured cells. We then examined the binding of the different ArtB mutants in a customized glycan array. We found that the ArtB^{S45A} mutant exhibited less residual glycan-binding activity than ArtB^{S31A} (Supplementary Fig. 12 and Supplementary Table 3), indicating that the ArtB^{Ser45} site plays a more prominent role in glycan binding. Importantly, comparison of the binding profiles of the ArtB^{S31A} and ArtB^{S45A} mutants indicated that the ArtB^{Ser45} site exhibits binding preference for glycans terminated in Neu5Ac-α2-6Gal/GalNAc (Supplementary Fig. 13 and Supplementary Table 4), a binding specificity absent in PltB[13]. Furthermore, we found that both ArtB mutants retained the ability to bind Neu5Gc-terminated glycans, indicating that both sites contribute to this expanded binding specificity (Supplementary Fig. 14 and Supplementary Table 5). To further explore the impact of delivering the typhoid toxin-associated toxic activities through the different ArtB glycan-binding sites, we assembled chimaeric toxins consisting of wild-type and different mutants of ArtB (ArtB^{S31A}, ArtB^{S45A} or ArtB$^{S31A/S45A}$) in complex with PltA and CdtB (Supplementary Fig. 15) and tested their toxic and binding activities in cultured human (displaying Neu5Ac-terminated glycans) and mouse (displaying Neu5Gc- and Neu5Ac-terminated glycans) cells. We found that, relative to one another, PltB exhibited greater binding to human cells, while ArtB exhibited higher binding to mouse cells (Fig. 4a). Although the chimaeric and typhoid toxins exhibited similar toxic activity to mouse cells (Fig. 4b and Supplementary Fig. 16), typhoid toxin showed more toxicity towards human cells (Fig. 4b). We also found that both ArtB glycan-binding sites played an important role in toxin delivery, because each of the individual mutants exhibited a significant reduction in toxicity, and simultaneous introduction of mutations in both sites resulted in the complete loss of toxicity (Fig. 4c). Taken together, these results indicate that the presence of an additional glycan-binding site broadens the glycan-binding specificity of ArtB relative to PltB.

We compared the toxicity of typhoid toxin with that of the ArtB/PltA/CdtB chimaera in an animal model of intoxication. Despite equivalent in vitro toxic activity (Fig. 4b and Supplementary Fig. 16), administration of the same amount of toxin to C57BL/6 mice resulted in a more rapid death in animals receiving typhoid toxin than those receiving the ArtB/PltA/CdtB chimaera toxin (Supplementary Fig. 17). Because Cmah expression in C57BL/6 mice is variable, these mice display both Neu5Ac- and Neu5Gc-terminated glycans[20]. We therefore compared the toxicity of the different toxin preparations in *Cmah*$^{-/-}$ mice, which display Neu5Ac-terminated human-like sialoglycans[20]. In addition, we constructed a transgenic mouse that constitutively expresses *Cmah* under a strong promoter and therefore almost exclusively displays Neu5Gc-terminated glycans (Fig. 4d,e and Supplementary Figs. 18 and 19). We found that, as predicted by its expanded glycan-binding specificity, the chimaeric ArtB/PltA/CdtB toxin displayed toxicity to the

Cmah transgenic mice, while, as predicted by its binding specificity[13], typhoid toxin did not (Fig. 4f,g). Surprisingly, however, despite its expanded binding specificity, the chimaeric toxin exhibited significantly less lethality than typhoid toxin for *Cmah*$^{-/-}$ mice. Furthermore, there were clear differences in the course of intoxication, as the mice receiving the ArtB/PltA/CdtB chimaeric toxin

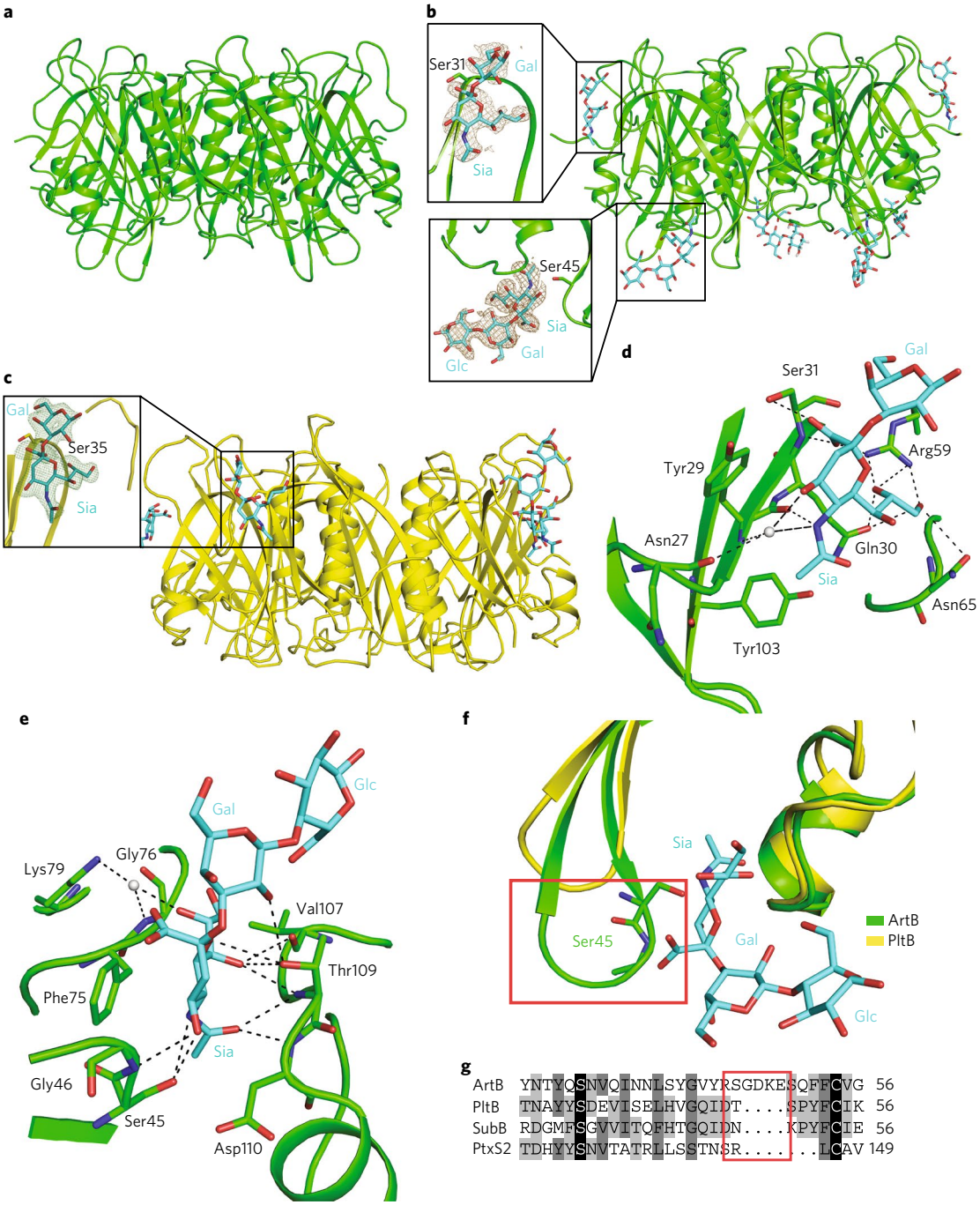

Fig. 3 | The atomic structure of ArtB bound to its receptor shows the presence of an additional glycan-binding site. a, Atomic structure of the ArtB pentamer shown as a ribbon cartoon. **b**, Atomic structure of the ArtB pentamer in complex with the Neu5Acα2-3Galβ1-4Glc oligosaccharide shown as a ribbon cartoon. Cyan, blue and red sticks represent carbon, nitrogen and oxygen atoms in the sugar backbone. Insets: close-up views of Neu5Acα2-3Galβ 1-4Glc and Neu5Acα2-3Gal. Brown mesh represents the sugar composite annealed omit difference density map contoured at 2.0σ. **c**, Atomic structure of the PltB pentamer in complex with the Neu5Acα2-3Gal oligosaccharide, shown as a ribbon cartoon. Cyan, blue and red sticks represent carbon, nitrogen and oxygen atoms in the sugar backbone. Insets: close-up views of Neu5Acα2-3Galβ1-4Glc. Green mesh represents the sugar composite annealed omit difference density map contoured at 2.5σ. **d**,**e**, Interactions between ArtB^{Ser31} (**d**) and ArtB^{Ser45} (**e**) with Neu5Acα2-3Gal and Neu5Acα2-3Galβ1-4Glc, respectively. ArtB is shown as a green ribbon cartoon, the sugar and amino acids interacting with the sugar are shown as sticks, the interactions are shown as black dashes and water is shown as grey balls. **f**, Structural comparison of ArtB^{Ser45} sugar-binding site with the equivalent surface in PltB. Blue and red sticks in the sugar backbone represent nitrogen and oxygen atoms, respectively. **g**, Amino-acid sequence alignment of ArtB^{Ser45} glycan-binding site with the equivalent regions in PltB, SubB and PtxS2. Red boxes in **f** and **g** highlight the insert sequence and the associated structural features that are uniquely present in ArtB.

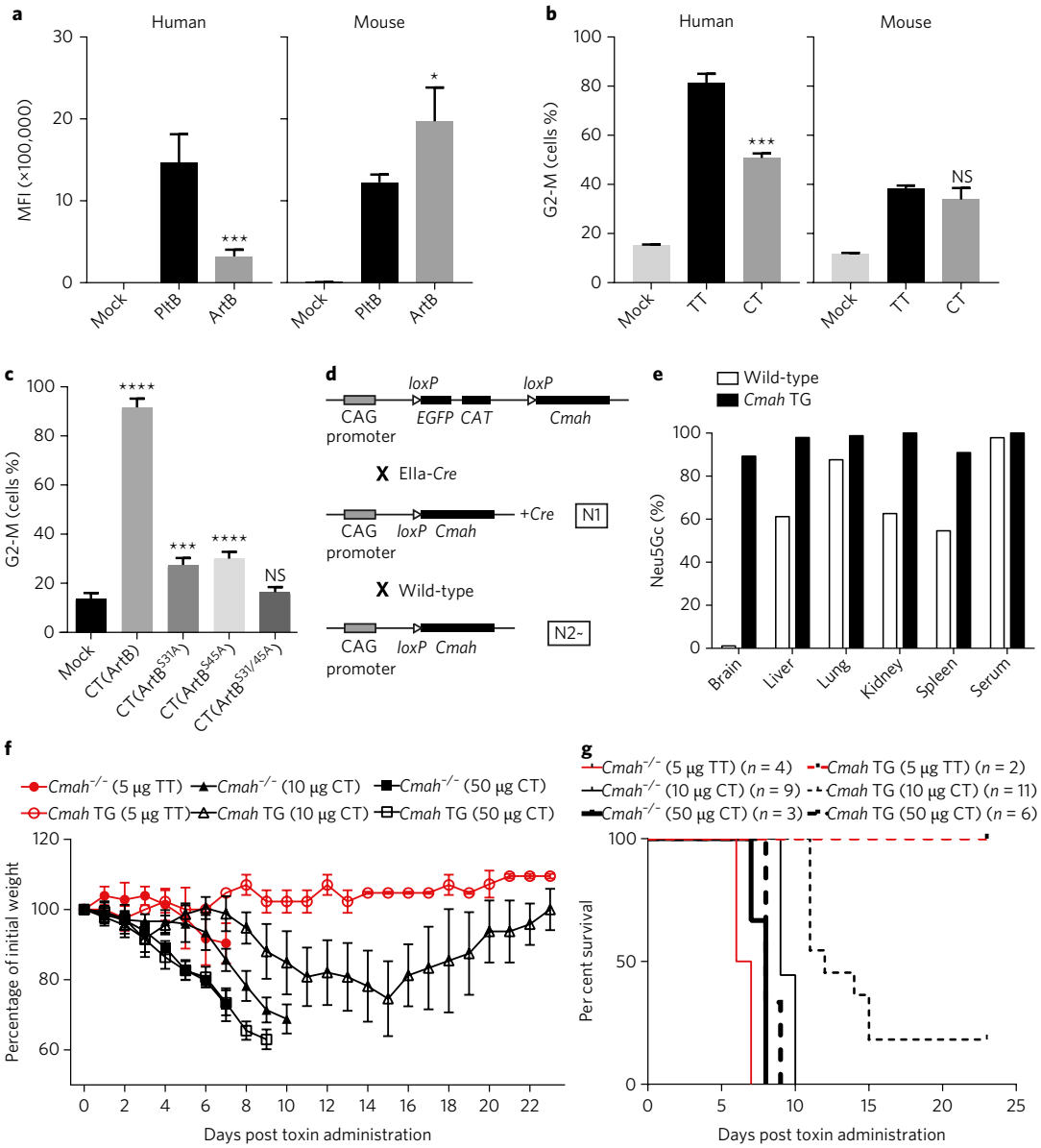

Fig. 4 | The ArtB/PltA/CdtB chimaeric toxin exhibits reduced lethality in mice relative to typhoid toxin. a, ArtB and PltB (2.5 μM each) binding to human (Henle-407) or mouse (embryo fibroblasts) cells. The binding of fluorescently labelled PltB and ArtB was evaluated by flow cytometry. The *y*-axis values represent the mean fluorescence index (MFI) and are the mean ± s.d. of at least three independent measurements. $^{*}P < 0.05$; $^{***}P < 0.0005$. **b**, Relative toxicity to human (Henle-407) or mouse (embryo fibroblasts) cells of purified typhoid toxin (TT) (3 pM) and ArtB/PltA/CdtB chimaeric toxin (CT) (3 pM). The percentage of cells in G2/M, a measure of CdtB toxic activity, after application of the indicated toxins, was determined by flow cytometry. Data are the mean ± s.d. of at least three independent determinations. $^{***}P < 0.0005$; NS (not significant), $P > 0.05$ compared to untreated cells. **c**, Relative contribution of the different ArtB glycan-binding sites to toxicity. Different ArtB/PltA/CdtB CT preparations containing the indicated ArtB mutants were tested for their ability to intoxicate cultured cells. Equal amounts (250 pM) of chimaeric toxin preparations were applied to the cultured cells and the percentage of cells in G2/M was determined by flow cytometry. Data are the mean ± s.d. of at least three independent determinations. $^{****}P < 0.0001$; $^{***}P < 0.0005$, NS, $P > 0.05$ compared to untreated cells. In **a**–**c**, two-tailed Student's *t*-tests were performed to determine the statistical significance for two group comparisons. **d**, Scheme of the strategy used to generate a *Cmah* TG mouse. Targeted Cre-inducible *Cmah* TG mice (transgene insertion in H11 locus, top) were crossed with EIIa-*Cre* mice that induce Cre expression at the pre-implantation embryo stage, and the resulting N1 generation mouse with the *Cmah* transgene and *Cre* was further mated with wild-type mice. Among the resulting N2 generation, the mice that had the *Cmah* transgene but lacked *Cre* were selected as systemic *Cmah* TG mice and maintained by crossing with wild-type mice. **e**, Tissue homogenates obtained from 11-week-old male mice were hydrolysed in 2 M acetic acid to release sialic acids after treatment with 0.1 M sodium hydroxide to remove *O*-acetylation of sialic acids. The percentage of Neu5Gc in total sialic acids was determined by high-performance liquid chromatography using a DMB (1,2-diamino-4,5-methylenedioxybenzene)-derivatization method. Each bar represents the average of samples from two mice per genotype. *Cmah* TG mice showed remarkably high Neu5Gc expression in all tissues tested. **f**,**g**, Mouse toxicity of the ArtB/PltA/CdtB chimaeric toxin relative to typhoid toxin. *Cmah*$^{-/-}$ or *Cmah* transgenic (TG) mice were administered intraorbitally either typhoid toxin (TT) (5 μg) or ArtB/PltA/CdtB chimaeric toxin (CT) (10 or 50 μg) and their body weight (**f**) and survival (**g**) at the indicated times were recorded. Values in **f** are presented as mean and s.d. The difference in weight loss between groups (**f**) was analysed by the Mann–Whitney test (TT versus CT in *Cmah* TG, $P < 0.0001$; TT versus CT in *Cmah*$^{-/-}$, $P < 0.05$). The difference in survival (**g**) was analysed by the Mantel Cox test (TT versus CT in *Cmah* TG, $P < 0.05$; TT (5 μg) versus CT (10 μg) in *Cmah*$^{-/-}$, $P < 0.001$.

did not show signs of stupor, but this was readily apparent in mice that received typhoid toxin. In contrast, leukopenia was apparent in all mice regardless whether they received typhoid toxin or the chimaeric toxin (Supplementary Fig. 20). These results indicate that, although typhoid toxin has narrowed its receptor-binding specificity, the process of host adaptation has resulted in heightened toxicity, presumably by gaining efficiency in the targeting of specific tissues and/or in its escape from soluble sialylated decoy ligands[21].

Taken together, this study indicates that typhoid toxin may have evolved from an ArtAB-like ancestor in at least two steps. One step involved the incorporation of an additional active subunit to an already existing AB_5 toxin by evolving specifically positioned Cys residues to coordinate the linking of PltA to CdtB by a disulfide bond. The interface between PltA and CdtB buries only ~950 Å^2, and CdtB is released from the toxin under reducing conditions, indicating that the disulfide bond is all that maintains the tethering of these two subunits to one another. Indeed, simply adding a terminal Cys residue to a CdtB homologue from a *S. diarizonae* CDT was sufficient to form a functional complex with ArtAB. The other step may have involved the narrowing and optimization of its glycan-binding site to maximize the toxin's effectiveness in its human host. In fact, the locus that encodes a typhoid toxin homologue in *S. diarizonae* contains two *pltB* homologues, *pltB*$^{Sdiar\text{-}1}$, which exhibits very close amino-acid and structural similarity to *S.* Typhi PltB, and *pltB*$^{Sdiar\text{-}2}$, a more divergent homologue that is more related to ArtB (Supplementary Figs. 21–24). Notably, we found that, unlike typhoid toxin, chimaeric toxins assembled with either of these homologues were able to intoxicate cells displaying either Neu5Ac- or Neu5Gc-terminated glycans (Supplementary Figs. 25 and 26). However, a chimaeric toxin assembled with *pltB*$^{Sdiari\text{-}1}$ exhibited more toxicity to cells displaying Neu5Ac-terminated glycans, while a chimaeric toxin assembled with *pltB*$^{Sdiari\text{-}2}$ showed the opposite preference (Supplementary Figs. 25 and 26). It is therefore possible that PltB$^{Sdiari\text{-}1}$ and PltB$^{Sdiari\text{-}2}$ represent an intermediate step in the evolution of *S.* Typhi's PltB from an ArtB-like ancestor. In summary, these findings describe a remarkable example of virulence factor evolution in which relatively minor genetic changes coupled to horizontal gene exchange within the same bacterial species may have led to the emergence of a powerful toxin exquisitely adapted to the human host.

Methods

Toxin expression and purification. Coding sequences for *artA* and *artB* were amplified from *S. enterica* serovar Typhimurium DT104 genomic DNA and cloned into the expression vector pET28b. Coding sequences for *pltB* homologues from *S. diarizonae* were amplified directly from bacterial cell lysates and cloned into the expression vector pET28b. Expression and purification of ArtB, ArtB chimaeric toxin, PltB^{sdiar} chimaeric toxin and typhoid toxin were carried out as previously described[6]. Plasmids expressing ArtB point mutations were constructed using standard recombinant DNA techniques.

Crystallization. The expression and purification of C-terminal His_6-tagged ArtB and PltB used for crystallization have been described previously[6]. Full-length ArtB protein (5 mg ml^{-1}) was used to perform initial spare matrix crystal screening with a crystallization robot at the Yale University School of Medicine Structural Biology Core facility. After optimization trials, the ArtB crystals were grown at room temperature using the hanging-drop vapour-diffusion method, mixing 1 µl protein with 1 µl reservoir solution consisting of 44% (wt/vol) PEG200, 0.1 M calcium chloride and 0.1 M MES, pH 5.5. Crystals appeared in ~3 days and matured in ~1 week. To obtain 3′-sialyllactose (3′SL)-bound ArtB crystals, purified ArtB protein was mixed with 5 mM 3′SL before setting up crystallization trays. The crystals used to collect diffraction data were grown in the presence of 35% (wt/vol) PEG200, 0.1 M calcium chloride and 0.1 M MES buffer, pH 5.5. To grow 3′SL-bound PltB crystals, purified protein was mixed 5 mM of 3′SL in the presence of 26% (wt/vol) PEG1500, 0.1 M sodium acetate, pH 4.6.

X-ray data collection and structure determination. X-ray data were collected at a wavelength of 1.5418 Å on a Rigaku Homelab system at the Yale University Chemical and Biophysical Instrumentation Center (http://cbic.yale.edu) or at the Yale University School of Medicine X-ray Crystallography Core Facility. Data were integrated and scaled using the HKL-2000[22] or Mosflm [23] software packages. Further processing was performed with programs from the CCP4 suite. The apo and 3′SL bound ArtB and PltB structures were determined by molecular replacement using PHASER[24] with the atomic coordinates of PltB (Protein Data Bank (PDB) ID 4RHR) as the initial search model. To complete the model, manual building was carried out in COOT. Figures were prepared using PyMol[25]. Structure refinement was done by PHENIX[26]. The data collection and refinement statistics are summarized in Supplementary Table 6. Coordinates for the atomic structures have been deposited in the RCSB PDB under numbers 5WHV, 5WHT and 5WHU (pending; http://www.rcsb.org/pdb/explore.do?structureId=4RHS).

Alexa 555 and Oregon Green 488 labelling. Purified wild-type PltB, ArtB and different ArtB mutants were fluorescently labelled with Alexa-555 or Oregon Green 488 (OG488, Invitrogen) according to the vendor's instructions. Purified PltB, ArtB and its mutants (2 mg ml^{-1} in 500 µl of 20 mM HEPES buffer, pH 8.1) were incubated for 1 h at room temperature with reactive dyes, and applied to the desalt spin columns to separate dye–protein conjugates from the free dyes.

Glycan microarray analysis. Glycan microarray analysis was carried out as previously described[13]. Briefly, glycan microarrays were fabricated using epoxide-derivatized glass slides, as previously described[27]. Printed glycan microarray slides were blocked by ethanolamine, washed and dried, and then fitted in a multiwell microarray hybridization cassette (ArrayIt) to divide into subarrays. The subarrays were blocked with ovalbumin (1% wt/vol) in PBS (pH 7.4) for 1 h at room temperature in a humid chamber with gentle shaking. Subsequently, the blocking solution was discarded, and the appropriate dilutions of the different Alexa Fluor 555-labelled protein samples (64 µg ml^{-1}) were added to each subarray. After incubation for 2 h at room temperature with gentle shaking, the slides were extensively washed to remove nonspecifically bound proteins. The developed glycan microarray slides were then dried and subjected to scanning by a Genepix 4000B microarray scanner (Molecular Devices). Data analysis was carried using the Genepix Pro 7.0 analysis software (Molecular Devices).

Mammalian cell culture conditions. Henle-407 human intestinal epithelial cells (Roy Curtiss Laboratory Collection), HEK293T cells, mouse-embryo fibroblasts (MEFs) and NIH3T3 cells (from the American Type Culture Collection) were cultured in DMEM containing 10% fetal bovine serum (FBS) at 37 °C in a cell culture incubator with 5% CO_2. All cell lines were routinely tested for the presence of mycoplasma using a standard PCR method. The cells were frequently checked for their morphological features, growth characteristics and functionalities, but were not authenticated by short tandem repeat (STR) profiling. Cells were split into 12-well plates at a cell density of 2.5×10^4 cells per well for the intoxication assays or at 2×10^5 cells per well for the toxin-binding assay. The next day, the cells were used for the different assays as described in the following.

Metabolic incorporation of Neu5Ac or Neu5Gc. Metabolic incorporation of Neu5Ac or Neu5Gc was carried out as previously described[13]. Briefly, a stock solution containing 50 mM Neu5Ac or Neu5Gc was freshly prepared in DMEM medium, pH 7.0. Henle-407 cells (1.5×10^5) were seeded onto 6-well culture plates in 3 ml medium containing 10 mM Neu5Ac or Neu5Gc. During the feeding period, the cells were continuously monitored and maintained below 80% confluence. After 3 days of growth, the cells were collected and seeded onto 12-well plates at a cell density of 2.5×10^4 cells per well in 1 ml medium containing 10 mM Neu5Ac or Neu5Gc. The next day, the cells were used for intoxication assays, as described in the following.

Toxin binding assay. Cultured cells were seeded in 12-well plates, and 16 h later were treated with different preparations of OG488-labelled PltB, ArtB or its mutants in Hank's Balanced Salt Solution for 30 min on ice. Cells were then washed three times with PBS, fixed with 2% paraformaldehyde, and ~10,000 cells were analysed by fluorescence-activated cell sorting (FACS) on a BD Accuri C6 flow cytometer. The toxin binding profile was then analysed using FlowJo cytometry software (Tree Star) (Supplementary Fig. 27). When indicated, cells were treated with 2 µl protein deglycosylation mix (NEB #P6039S; contains PNGase F, *O*-glycosidase, neuraminidase, β1–4 galactosidase and β-*N*-acetylglucosaminidase) or 50 units of α2-3,6,8 neuraminidase (NEB#P0720S) and incubated for 2 h at 37 °C before toxin-binding assay and flow cytometric analyses.

Mammalian cell intoxication assay. Cell cycle arrest after intoxication by the ArtB chimaeric or typhoid toxins was examined by flow cytometry as previously described[28]. Briefly, cells were treated with the different toxin preparations and, 66 h (for Henle-407) or 48 h (for NIH3T3) after treatment, cells were trypsinized, collected, washed and fixed overnight in ~70% ethanol/PBS at −20 °C. Fixed cells were washed with PBS and resuspended in 500 µl of PBS containing 50 µg ml^{-1} propidium iodide, 0.1 mg ml^{-1} RNase A, and 0.05% Triton X-100. After incubation for 30 min at 37 °C, cells were washed with PBS, resuspended in 500 µl PBS, filtered and analysed (3,000–5,000 cells) by a flow cytometry on a BD Accuri C6 flow cytometer. The DNA content of treated cells was determined using FlowJo software (Supplementary Fig. 28).

Generation of a Neu5Gc-overexpressing *Cmah* transgenic mouse. A *Cmah* transgenic mouse overexpressing Neu5Gc was generated following standard approaches following the scheme depicted in Fig. 4.

Mouse intoxication experiments. Mouse lines have been previously described[13], and all animal experiments were conducted according to protocols approved by Yale University's Institutional Animal Care and Use Committee. Seven- to ten-week old C57BL/6, *Cmah*$^{-/-}$ or *Cmah* transgenic (TG) mice were anaesthetized with 30% wt/vol isoflurane in propylene glycol and 100 µl of toxin solution was administered via the retro-orbital route. Changes in behaviour, weight and survival of the toxin-injected mice were closely monitored for the duration of the experiment. Blood samples were collected by cardiac puncture 4 days after toxin administration in Microtainer tubes coated with EDTA, kept at room temperature, and analysed within 2 h of blood collection using a HESKA Veterinary Hematology System. The number of animals used in each experiment was determined empirically using prior experience with equivalent types of experiment.

Structural modelling. Structural modelling was performed online using the SWISS-MODEL Server (https://swissmodel.expasy.org) with the PltB structure (PDB ID 4RHR) as template. The highest scored structure was selected for structural comparisons.

Statistical analysis. Mice were randomly allocated to different groups. Investigators were not blinded to the allocation during the experiments or to the outcome assessment. Two-tailed Student's *t*-tests were performed to determine the statistical significance for two group comparisons. Given the nature of the experiments and the types of sample, mouse weight loss was assessed with a non-parametric Mann–Whitney test and mouse survival was assessed with a Mantel Cox test (log-rank test). A p value of <0.05 was considered to be statistically significant. All analyses were performed using GraphPad Prism (GraphPad software).

Data availability. The data that support the findings of this study are available from the corresponding author upon request. Coordinates for the atomic structures have been deposited in the RCSB Protein Data Bank under PDB codes 5WHV, 5WHU and 5WHT.

Received: 12 March 2017; Accepted: 23 August 2017;
Published online: 9 October 2017

References

1. Jackson, R., Johnson, L., Clarke, S. & Arnold, D. Bacterial pathogen evolution: breaking news. *Trends Genet.* **27**, 32–40 (2011).
2. Donnenberg, M. S. & Whittam, T. S. Pathogenesis and evolution of virulence in enteropathogenic and enterohemorrhagic *Escherichia coli*. *J. Clin. Invest.* **107**, 539–548 (2001).
3. Bentley, S. & Parkhill, J. Genomic perspectives on the evolution and spread of bacterial pathogens. *Proc. Biol. Sci.* **282**, 20150488 (2015).
4. Alizon, S. & Michalakis, Y. Adaptive virulence evolution: the good old fitness-based approach. *Trends Ecol. Evol.* **30**, 248–254 (2015).
5. Daugherty, M. & Malik, H. Rules of engagement: molecular insights from host–virus arms races. *Annu. Rev. Genet.* **46**, 677–700 (2012).
6. Song, J., Gao, X. & Galan, J. E. Structure and function of the *Salmonella* Typhi chimaeric A_2B_5 typhoid toxin. *Nature* **499**, 350–354 (2013).
7. Galán, J. Typhoid toxin provides a window into typhoid fever and the biology of *Salmonella* Typhi. *Proc. Natl Acad. Sci. USA* **113**, 6338–6344 (2016).
8. Parry, C., Hien, T. T., Dougan, G., White, N. & Farrar, J. Typhoid fever. *N. Engl. J. Med.* **347**, 1770–1782 (2002).
9. Crump, J. & Mintz, E. Global trends in typhoid and paratyphoid fever. *Clin. Infect. Dis.* **50**, 241–246 (2010).
10. Raffatellu, M., Wilson, R., Winter, S. & Bäumler, A. Clinical pathogenesis of typhoid fever. *J. Infect. Dev. Ctries* **2**, 260–266 (2008).
11. Wain, J., Hendriksen, R., Mikoleit, M., Keddy, K. & Ochiai, R. Typhoid fever. *Lancet* **385**, 1136–1145 (2015).
12. Dougan, G. & Baker, S. *Salmonella enterica* serovar Typhi and the pathogenesis of typhoid fever. *Annu. Rev. Microbiol.* **68**, 317–336 (2014).
13. Deng, L. et al. Host adaptation of a bacterial toxin from the human pathogen *Salmonella* Typhi. *Cell* **159**, 1290–1299 (2014).
14. Varki, N., Strobert, E., Dick, E. J., Benirschke, K. & Varki, A. Biomedical differences between human and nonhuman hominids: potential roles for uniquely human aspects of sialic acid biology. *Annu. Rev. Pathol.* **6**, 365–393 (2011).
15. Saitoh, M. et al. The artAB genes encode a putative ADP-ribosyltransferase toxin homologue associated with *Salmonella enterica* serovar Typhimurium DT104. *Microbiology* **151**, 3089–3096 (2005).
16. Lara-Tejero, M. & Galan, J. E. Cytolethal distending toxin: limited damage as a strategy to modulate cellular functions. *Trends Microbiol.* **10**, 147–152 (2002).
17. Desai, P. et al. Evolutionary genomics of *Salmonella enterica* subspecies. *mBio* **4**, e00579-12 (2013).
18. Wang, C. et al. Complete genome sequence of *Salmonella enterica* subspecies *arizonae* str. RKS2983. *Stand. Genomic Sci.* **10**, 30 (2015).
19. Byres, E. et al. Incorporation of a non-human glycan mediates human susceptibility to a bacterial toxin. *Nature* **456**, 648–652 (2008).
20. Hedlund, M. et al. *N*-glycolylneuraminic acid deficiency in mice: implications for human biology and evolution. *Mol. Cell. Biol.* **27**, 4340–4346 (2007).
21. Beddoe, T., Paton, A., Le Nours, J., Rossjohn, J. & Paton, J. Structure, biological functions and applications of the AB5 toxins. *Trends Biochem. Sci.* **35**, 411–418 (2010).
22. Otwinowski, Z. & Minor, W. Processing of X-ray diffraction data collected in oscillation mode. *Methods Enzymol.* **276**, 307–326 (1997).
23. Winn, M. D. et al. Overview of the CCP4 suite and current developments. *Acta Crystallogr. D Biol. Crystallogr.* **67**, 235–242 (2011).
24. McCoy, A. J. et al. Phaser crystallographic software. *J. Appl. Crystallogr.* **40**, 658–674 (2007).
25. DeLano, W. L. The PyMOL molecular graphics system (Schrödinger, 2002); http://www.pymol.org
26. Adams, P. D. et al. PHENIX: a comprehensive Python-based system for macromolecular structure solution. *Acta Crystallogr. D Biol. Crystallogr.* **66**, 213–221 (2010).
27. Padler-Karavani, V. et al. Rapid evolution of binding specificities and expression patterns of inhibitory CD33-related Siglecs in primates. *FASEB J.* **28**, 1280–1293 (2014).
28. Spano, S., Ugalde, J. E. & Galan, J. E. Delivery of a *Salmonella* Typhi exotoxin from a host intracellular compartment. *Cell Host Microbe* **3**, 30–38 (2008).

Acknowledgements

The authors thank J. Wang for suggestions and for providing help with structure refinement, and the Galan Laboratory for careful review of the manuscript. G.S. is supported in part by a Postdoctoral Fellowship from the EMBO (ALTF 172-2015). Crystal screening was conducted at the Yale Macromolecular X-ray Core Facility (1S10OD018007-01). This work was supported by National Institutes of Health grants AI079022 (to J.E.G.) and GM32373 (to A.V.).

Author contributions

X.G., G.S., L.D., A.V. and J.E.G. designed the research and analysed data. X.G., G.S. and L.D. performed the research. Y.N.-M., H.Y. and X.C. provided critical reagents. X.G. and J.E.G. wrote the manuscript with input from all the authors.

Competing interests

The authors declare no competing financial interests.

Additional information

Supplementary information is available for this paper at doi:10.1038/s41564-017-0033-2.

Correspondence and requests for materials should be addressed to J.E.G.

nature research

Corresponding author(s): Jorge E. Galan

☐ Initial submission ☒ Revised version ☐ Final submission

Life Sciences Reporting Summary

Nature Research wishes to improve the reproducibility of the work that we publish. This form is intended for publication with all accepted life science papers and provides structure for consistency and transparency in reporting. Every life science submission will use this form; some list items might not apply to an individual manuscript, but all fields must be completed for clarity.

For further information on the points included in this form, see Reporting Life Sciences Research. For further information on Nature Research policies, including our data availability policy, see Authors & Referees and the Editorial Policy Checklist.

Experimental design

1. Sample size

Describe how sample size was determined.

Sample sizes were empirically determined to optimize numbers based on our previous experience with equivalent experiments.

2. Data exclusions

Describe any data exclusions.

No data were excluded from the analyses

3. Replication

Describe whether the experimental findings were reliably reproduced.

All attempts at replicating the results were successful

4. Randomization

Describe how samples/organisms/participants were allocated into experimental groups.

Samples were randomly allocated to different groups

5. Blinding

Describe whether the investigators were blinded to group allocation during data collection and/or analysis.

Investigators were not blinded to group allocation during the experiments or to the outcome assessment.

Note: all studies involving animals and/or human research participants must disclose whether blinding and randomization were used.

6. Statistical parameters

For all figures and tables that use statistical methods, confirm that the following items are present in relevant figure legends (or in the Methods section if additional space is needed).

n/a	Confirmed
☐	☒ The exact sample size (*n*) for each experimental group/condition, given as a discrete number and unit of measurement (animals, litters, cultures, etc.)
☐	☒ A description of how samples were collected, noting whether measurements were taken from distinct samples or whether the same sample was measured repeatedly
☐	☒ A statement indicating how many times each experiment was replicated
☐	☒ The statistical test(s) used and whether they are one- or two-sided (note: only common tests should be described solely by name; more complex techniques should be described in the Methods section)
☐	☒ A description of any assumptions or corrections, such as an adjustment for multiple comparisons
☐	☒ The test results (e.g. *P* values) given as exact values whenever possible and with confidence intervals noted
☐	☒ A clear description of statistics including central tendency (e.g. median, mean) and variation (e.g. standard deviation, interquartile range)
☐	☒ Clearly defined error bars

See the web collection on statistics for biologists for further resources and guidance.

Software

Policy information about availability of computer code

7. Software

Describe the software used to analyze the data in this study.	GraphPad Prism 7

For manuscripts utilizing custom algorithms or software that are central to the paper but not yet described in the published literature, software must be made available to editors and reviewers upon request. We strongly encourage code deposition in a community repository (e.g. GitHub). *Nature Methods* guidance for providing algorithms and software for publication provides further information on this topic.

Materials and reagents

Policy information about availability of materials

8. Materials availability

Indicate whether there are restrictions on availability of unique materials or if these materials are only available for distribution by a for-profit company.	All unique materials used are readily available from the authors

9. Antibodies

Describe the antibodies used and how they were validated for use in the system under study (i.e. assay and species).	No antibodies were used

10. Eukaryotic cell lines

a. State the source of each eukaryotic cell line used.	HEK293T, MEF and NIH3T3 cells obtained from the American Type Culture Collection (ATCC). Henle-407 were from the Roy Curtiss laboratory collection
b. Describe the method of cell line authentication used.	The cells were frequently checked for their morphological features, growth speed and functionalities, but were not authenticated by short tandem repeat (STR) profiling.
c. Report whether the cell lines were tested for mycoplasma contamination.	All cell lines tested negative for mycoplasma contamination
d. If any of the cell lines used are listed in the database of commonly misidentified cell lines maintained by ICLAC, provide a scientific rationale for their use.	No commonly misidentified cell lines were used

Animals and human research participants

Policy information about studies involving animals; when reporting animal research, follow the ARRIVE guidelines

11. Description of research animals

Provide details on animals and/or animal-derived materials used in the study.	7 to 10-week C57BL/6, Cmah-/- or Cmah transgenic (TG) mice were used for the study

Policy information about studies involving human research participants

12. Description of human research participants

Describe the covariate-relevant population characteristics of the human research participants.	The study did not involve human research participants